

Influence of Aluminum Depletion Effects on the Calculation of the Oxidation Lifetimes of FeCrAl Alloys

I. G. Wright, R. Peraldi, and B. A. Pint

Oak Ridge National Laboratory, Oak Ridge, TN 37830-6156; wrightig@ornl.gov

Keywords: oxidation; ODS FeCrAl alloys; lifetime models; concentration profiles

Abstract. The oxidation behavior of FeCrAl-based alloys at temperatures in the range 1000 to 1300°C can be well described in terms that are readily quantified and so may be used for predicting their oxidation-limited lifetimes. These alloys rapidly establish a scale that is exclusively $\text{-Al}_2\text{O}_3$, which forms as a single, uniformly thick layer; when scale spallation occurs, the alumina layer is reformed with minimal formation of base-metal/transient oxide. This behavior is maintained until essentially all of the Al content of the alloy has been consumed, after which rapid ('breakaway') oxidation ensues. This well controlled oxidation behavior allows a straightforward approach for calculating oxidation lifetime by equating the total (available) alloy Al content with the rate of its consumption by oxidation. A simplifying assumption is that a flat Al depletion profile is maintained throughout, so that the minimum Al content at which breakaway occurs (C_{Bb}) is essentially zero. This paper presents experimental measurements of C_{Bb} for different specimen shapes, and explores possible reasons for the apparent effects of specimen shape on oxidation lifetime. The above assumptions appear reasonable for disc-shaped specimens, and values of $C_{Bb} = 0.001$ mass fraction were measured on specimens taken to failure. However, specimens of the same alloy with the same thickness (and/or same volume/surface area ratio) but different shapes were found to exhibit different oxidation lifetimes.

Introduction

Oxide dispersion-strengthened alloys have several features that require different considerations from conventional wrought high-temperature alloys when they are applied in practice. In particular, below some threshold load they exhibit an extremely low creep rate [1] so that, in the absence of inadvertent increase in loading, eventual failure is likely to result from environmental degradation. When exposed above approximately 1000°C in most environments, the ferritic FeCrAl-based ODS alloys form a thin, uniformly-thick protective scale of $\text{-Al}_2\text{O}_3$ that thickens very slowly with time. If such scales remain free from mechanical damage, eventual failure results from exhaustion of the Al content by consumption in the oxidation process; this mode of failure has been termed "chemical breakdown" [2]. Because the protective oxide is so thin, and because there is essentially no penetration of corrosion products into the alloy, it is virtually impossible to evaluate the remaining life of the FeCrAl substrate by non-destructive test methods based on thickness loss, so that some form of modeling based on understanding of the oxidation process is needed to assist life prediction.

The fact that these alloys exhibit such well-controlled oxidation behavior has allowed the application of relatively simple approaches for oxidation life modeling, based on knowledge of the rate of Al consumption from growth of the scale and of the total amount of Al available [3-7]. The most rudimentary form of this model is

$$\text{Lifetime} = (\text{Al available for oxide formation})/(\text{rate of Al consumption by oxidation}) \quad (1)$$

and the main parameters are the initial mass fraction of Al in the alloy (C_{B0}) and that at which a protective Al_2O_3 can no longer form (C_{Bb}), descriptors of the specimen size and shape (currently: surface area A , and volume, V), as well as the time- and temperature-dependence of the oxidation rate [1,7]. A key assumption is that the Al available for oxidation is ($C_{B0}-C_{Bb}$); this relies on the rate of Al diffusion in the alloy being much faster than the rate of Al consumption by oxidation, which appears to be the case above 1080°C [8], so that there is no development of an Al concentration gradient through

the alloy with time. Where chemical breakdown is assumed, the value of C_{Bb} is typically taken to be in the range of 0 to 0.001 [2,9,10], although values of 0.015-0.017 at 1200-1300°C [5,8] and 0.018 at 1350°C [11] also have been suggested.

Observations have indicated differences in oxidation lifetimes among alumina scale-forming alloys with similar values of C_{Bo} and V/A [12], where differences in substrate strength have allowed stress relief between the alloy and oxide by macro deformation of the specimen so that eventual failure was by chemical breakdown, or by scale spallation, resulting in accelerated consumption of Al and a mechanically-assisted chemical breakdown failure mode [2]. Also, differences have been observed in lifetimes among parallelepiped- and disc-shaped specimens of nominally the same size [1,10], and wedge-shaped specimens have exhibited lifetimes different than expected [11,13]. These results suggest different contributions of shape to localized scale spallation than are accounted for by the shape factor (V/A). The present study was undertaken to further understand the way in which specimen shape influences oxidation lifetime.

Experimental Procedures

The alloy studied was Inconel MA956®, which was supplied in the form of a 1.2 cm-thick flat bar by Special Metals Corp. (Huntington, West Virginia). The alloy composition is shown in Table 1. Specimens with parallelepiped and disc shapes, with nominal dimensions shown in Table 2, were electro-discharge machined from the bar. The dimensions were chosen to provide a direct comparison among specimens with the same thickness and shape factor (V/A) and, in the case of the short parallelepiped and disc, the same surface area and volume. Specimens were exposed with a 600 grit surface finish. Before exposure, individual specimens were measured to ± 0.01 mm using a digital micrometer, followed by degreasing in methanol and acetone, and weighing to ± 0.02 mg using a Mettler model AG245 balance. Specimens of each shape were exposed in individual,

Table 1. Alloy composition [wt%]

Batch No.	Fe	Ni	Co	Al	Cr	Ti	Y	C	Si	N	O	S	P	Mn
UBD0581	Bal	0.11	0.03	4.46	19.64	0.39	0.41	0.011	0.03	0.023	0.24	0.070	0.013	0.14

annealed, lidded alumina crucibles in laboratory air in a box furnace. Runs were initiated by inserting the loaded crucibles into the cold furnace, which was then heated to the test temperature of 1250°C over approximately 4 hours. At 100h intervals during the exposures, the power to the furnace was turned off and the specimens were furnace cooled and reweighed. At the conclusion of the tests, the macro-appearance of the specimens and the scale topography were examined by

Table 2. Nominal specimen dimensions (in mm)

Shape	Thickness	Length	Width	Surface area [mm ²]	Volume [mm ³]	V/A [mm]	Life [h]
Standard p'piped	1.6	23	12.5	689	461	0.67	1,500
Short p'piped	1.6	14	12.5	435	280	0.64	2,000
Disc	1.6	15		429	283	0.66	2,400

optical and scanning-electron microscopy (SEM), after which the specimens were mounted in epoxy, cross sectioned and metallographically polished to allow further examination by optical microscopy and electron-probe microanalysis (EPMA). Several sections were made from each specimen to explore the extent of any localized Al and Cr depletion at specimen edges and corners.

Results

Oxidation Kinetics. The total and specimen mass changes of specimens of each shape are shown in Fig. 1. One of each shape was exposed until breakaway oxidation initiated, while the other was removed from test immediately before breakaway. The total mass change data exhibited the expected parabolic

behavior [7], with the specimens taken to breakaway showing an increase in the rate of total mass gain approximately 200h before failure, and a sharp decrease in specimen mass at the point of breakaway, due to massive scale spallation on cooling. The observed oxidation lifetimes (listed later in Table 4) were taken as the point where the rate of total mass change increased sharply, indicative of a change in the protective nature of the scale. These values were different for the three shapes, in the order: disc > short parallelepiped > standard parallelepiped.

The appearance of the failed specimens after test is shown in Fig. 2. On the standard parallelepiped breakaway oxidation initiated at one corner whereas, on the short parallelepiped, breakaway appeared to have occurred more-or-less simultaneously around the specimen edges. On the disc the main scale had a more pronounced color change (from grey to orange-brown) than on the standard parallelepiped, indicating that the alloy Al content was exhausted and Cr and/or Fe had entered the scale. Although the scale spalled extensively from the disc on cooling after the final cycle, there was no formation of voluminous Cr- or Fe-rich oxide.

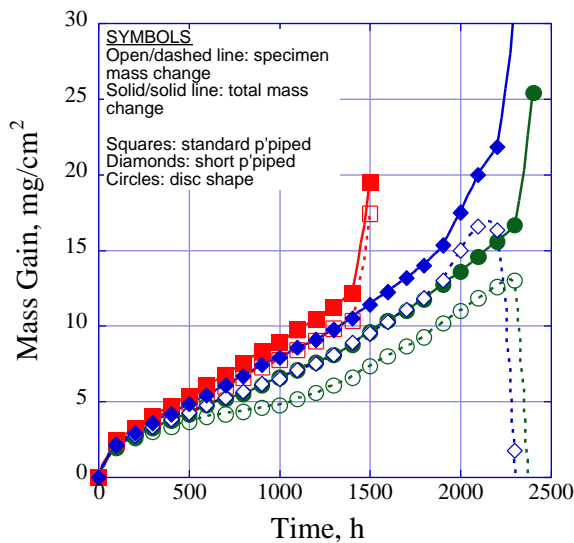


Figure 1. Oxidation kinetics of MA956 in air, 100h cycles at 1250°C. Data are shown for parallelepiped and disc shapes, taken to failure.

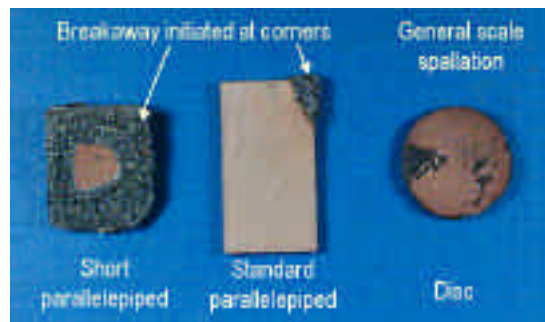


Figure 2. Macro plan views of scale failure on specimens of different shapes shown in Fig. 1.

Scale Morphologies. Figure 3 compares cross sections of the scales formed on the ends of two standard parallelepiped-shaped specimens exposed for 15 x 100h cycles (a) to failure, and (c) to the verge of failure. The corner at which scale failure occurred is indicated by track A in Fig. 3a, and the

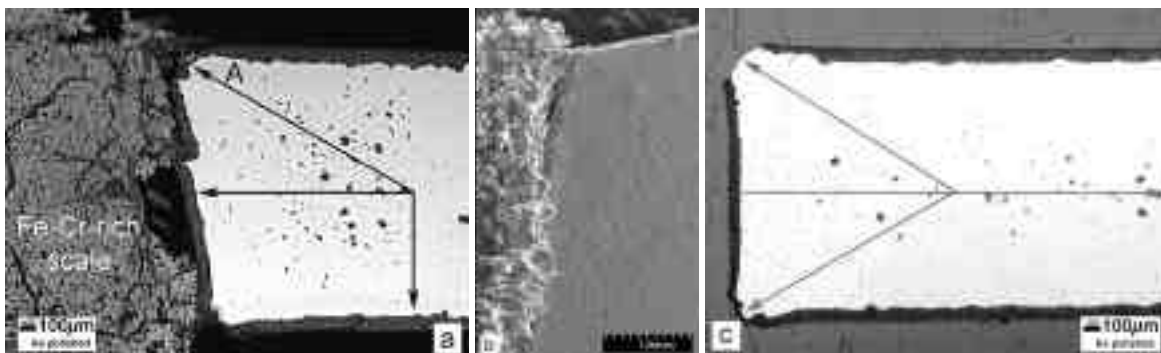


Figure 3. Cross sections of standard parallelepiped-shaped specimens exposed for 15 x 100h cycles at 1250°C (a) oxidized to failure (b) SEM image of the corner where breakaway oxidation initiated (c) immediately before failure. The lines drawn on the cross sections indicate the EPMA tracks.

voluminous, non-protective scale is clearly seen in section, and in plan view in Fig. 3b. Over the rest of the specimen, even at the same end as the failure, the morphology of the external scale was indistinguishable from that on the specimen that had not failed. Both specimens exhibited undulating metal-oxide interfaces, as well as clusters of large voids along the alloy centerline. One notable difference was the formation of internal precipitates of alumina and AlN (rod-shaped) near the failed end, shown in Fig. 3a. All four corners of each specimen showed signs of gross deformation.

Figure 4a shows a cross section through an edge of a short parallelepiped-shaped specimen that suffered breakaway oxidation. The voluminous scale at the specimen end was largely Fe-rich, with a Cr-rich area next to the alloy; the layer of precipitates in the alloy immediately ahead of the breakaway

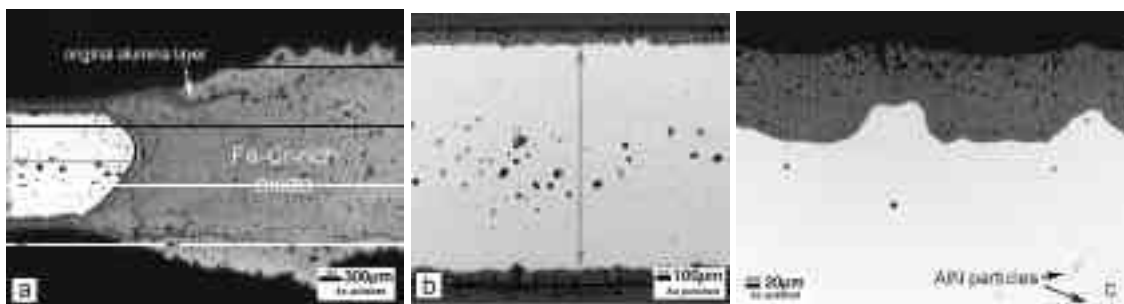


Figure 4. Cross sections of short parallelepiped-shaped specimens (a) failed after 23 x 100h cycles at 1250°C (b-c) immediately before failure after 19 x 100h cycles at 1250°C. The lines drawn on the cross sections indicate the tracks along which concentration profiles were measured.

oxidation front was Cr-rich. The inference is that the oxidation rate after breakaway was sufficiently fast that the Cr in the alloy was fixed as non-protective internal precipitates that were incorporated into the advancing oxidation front, rather than diffusing to the surface to form a continuous layer. The original protective alumina scale is evident as the darker, outer portion of the scale on the major faces of the specimen and separating the Fe-rich and Fe-Cr-rich regions of the voluminous scale (Fig. 4a). On the similar specimen on the verge of breakaway oxidation after 19 x 100h cycles, the metal-oxide interface had become undulating (Fig. 4b), an apparently continuous layer of Cr-rich oxide was growing beneath the alumina (Fig. 4c), and internal precipitates of AlN had formed near the alloy surface (arrow in Fig. 4c). The cracking in the outer part of the alumina scale over the high-points of these undulations may be a precursor to mechanical breakdown.

Figure 5a shows a cross section through an edge of a disc specimen oxidized until breakaway occurred. The scale on the major faces had formed a thick, Cr-rich subscale which was being further oxidized to form a wedge of Fe-Cr oxide that separated the main scale from the substrate. In addition, there were

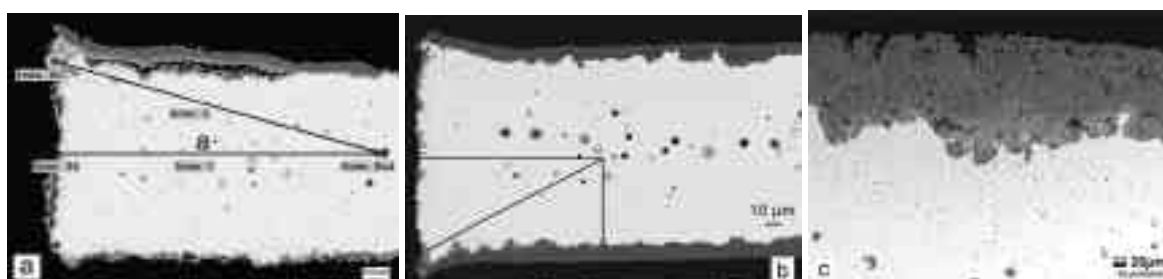


Figure 5. Cross sections of disc-shaped specimens (a) failed after 23 x 100h cycles at 1250°C (b-c) immediately before failure after 20 x 100h cycles at 1250°C. The lines drawn on the cross sections indicate the tracks along which concentration profiles were measured.

numerous fine precipitates of AlN particles (rod shapes) as well as discrete alumina particles immediately beneath the main scale and large voids along the alloy core. Cross sections from a similar specimen that was oxidized to the verge of breakaway oxidation are shown in Figs. 5b and c. These also show the presence of a significant Cr-rich subscale, cracking in the outer scale, internal rod-shaped particles (Fig. 5c). Furthermore, the scale from the specimen end had spalled. In some locations, separation had initiated between the Cr-rich subscale and the external Al-rich scale.

Concentration Profiles. Figure 6 shows the locations of the tracks along which EPMA concentration gradients were measured on cross sections. Profiles for Al, Cr, and Fe were measured from the specimen centerline axially to the specimen end; transversely to one of the major faces of the specimen; and diagonally into the corner or edge.



Figure 6. Schematic locations of the tracks of EPMA concentration profiles

Standard Parallelepiped-Shaped Specimens: Figure 7a indicates the results for the section into a failed corner; the diagonal traverse shows that the Al level at the failed corner was 0.24% (all concentrations are given in weight percent), rising to 1.70% over 5 mm toward the center of the specimen. Over the same traverse, the Cr content was 21.97 and 21.03%, respectively (Table 3), indicating that Cr consumption by oxidation had not started. The axial traverse from the non-failed scale adjacent to the failed corner showed Al and Cr profiles that closely tracked those into the corner (Fig. 7a), but with 0.63% Al and 21.85% Cr immediately subjacent to the intact scale, rising to 1.61% Al and 21.22% Cr over 5 mm. Much shallower Al concentration gradients were measured in the axial section: the diagonal traverse indicated 0.52% Al at the specimen edge, and the axial traverse showed an Al level at

Table 3. Summary of Measured Metal-Oxide Interface Al Concentrations

Specimen	Location of Analysis	Concentration [wt%]			
		Immediately before failure		Failed specimen	
		Al	Cr	Al	Cr
Standard p'piped	center	1.3	21.1	1.61-2.10	20.9-21.3
	major face			1.53-2.06	21.3-21.4
	end	1.2	21.2	0.63-1.82	21.1-21.9
	corner (edge)	(1.1-1.2)	(21.2)	0.24 (1.77)	22.0 (21.7)
<i>Non-failed end</i>	center			1.94	20.9
	end			1.50	21.1
Short p'piped	center	0.1	21.2	0.1	19.3-19.5
	major face	0-0.1	21.1-21.2	0.0-0.1	18.1-21.2
	end			0.1	6.1
Disc	center	0.1	20.7-20.9	0.06-0.09	19.1-20.0
	major face	0.1	20.3-20.6	0.04-0.05	18.3-19.2
	end	0.0-0.1	18.8	0.05	13.4
	edge	0.0	18.4	0.02	12.2

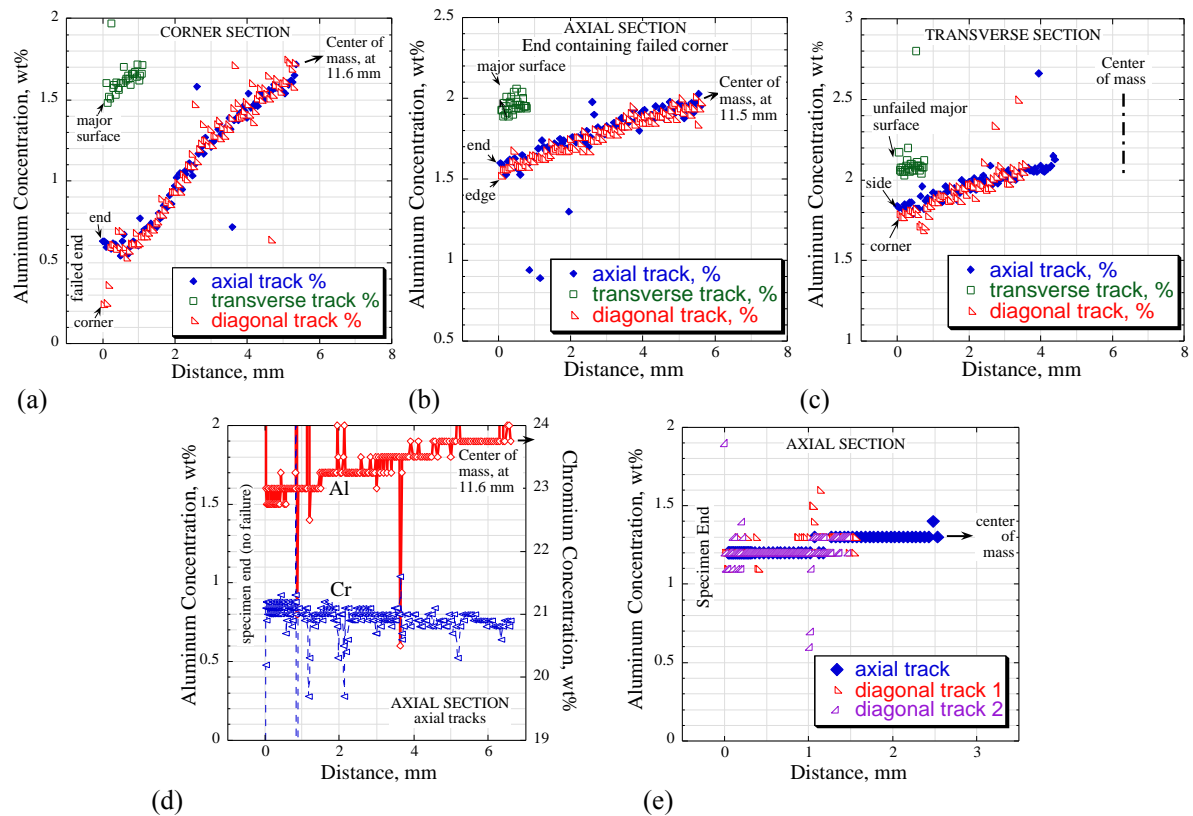


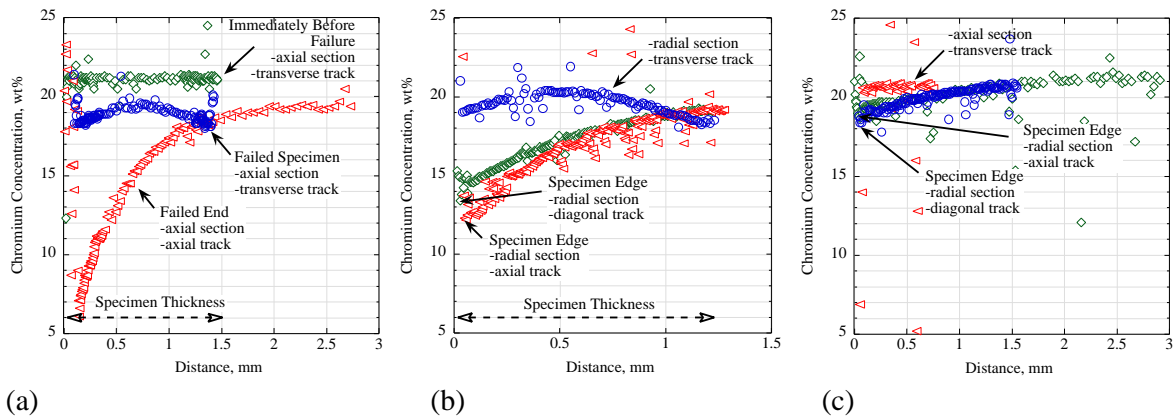
Figure 7. EPMA Al concentration profiles in standard parallelepiped-shaped specimens exposed for 15 x 100h cycles at 1250°C, oxidized to failure, (a) section into failed corner; (b) axial section to failed end; (c) transverse section; (d) axial section to non-failed end; and (e) specimen immediately before failure, axial section.

the end of 1.60, rising to 1.94 and 1.97, respectively, over 5.5 mm. The profiles through the axial section indicated 1.77% Al at the specimen edge, and 1.82% at the specimen side. In all three sections examined in Figs. 7a-c there was a slight Al gradient beneath the scale on the major faces, falling from 1.67 to 1.53% (diagonal traverse); 1.94 to 1.89% (axial traverse); and 2.08 to 2.06% (transverse).

There was less Al depletion at the end of the specimen opposite the failure, from 1.50% at the end to 1.94% over 6.5 mm in an axial section (Fig. 7d). Similar profiles for a specimen removed from test immediately before obvious failure indicated a much shallower Al gradient, from 1.20% at the end and 1.14-1.16% at the corners, to 1.30% over a distance up to 2.6 mm from (Fig. 7e).

Short Parallelepiped-Shaped Specimens: Concentration profiles measured along a center line of the failed specimen indicated that the Al content had been almost totally consumed (0.1%; Table 3); the Cr had been depleted to 6.1% (Fig. 8a). Concentration profiles across the specimen thickness away from edges indicated uniform consumption of the Al to 0 to 0.1% (with the higher Al peaks due to Al-rich internal oxide (or nitride) particles), as well as depletion of Cr to 18.1 % as a result of the formation of a basal layer of Cr-rich oxide (as detailed elsewhere [14]). In contrast, similar profiles across the thickness of the specimen removed from test immediately before breakaway indicated that, while the Al content had been uniformly decreased to 0-0.1%, and internal oxide and AlN precipitates were present (Fig. 5b), oxidation of Cr had not started (Table 3).

Disc-Shaped Specimens: Concentration profiles for a specimen oxidized to failure indicated that, for a distance of 1.5 mm to the specimen end, to an edge, and through the specimen thickness, the Al level of the alloy had been depleted uniformly to 0.1 wt%. The Cr profiles (Fig. 8b) suggest that consumption of Cr had initiated at a corner (hence the observed early spallation), but not on the major



(a) (b) (c)
Figure 8. Cr profiles along stated directions in (a) short parallelepiped; (b) failed disc; and (c) disc removed from test before failure.

faces. The Al level of the specimen removed from test before obvious failure (shown in Fig. 5b) also had been uniformly exhausted. From the specimen edge for a distance of 2.5 mm, the Al level was 0 to 0.1% (Table 3), while the Cr level rose from 18.4 to 20.7 (Fig. 8c). A similar Cr depletion was observed at the specimen end, but not beneath the scale on a major face near the center of the specimen (Fig. 8c).

Discussion

In these tests, scale failure typically initiated at corners on the standard and short parallelepipeds, and at the edges of the discs. Despite the limited number of specimens available at the time of reporting, there appeared to be an obvious differentiation among the times to failure of the studied shapes, with standard parallelepipeds failing earliest. During testing, semi-continuous spallation of a small amount of fine oxide was noted from the specimen ends of all the shapes, but the early failure of the standard parallelepipeds appeared to be associated with persistent scale spallation from corners. This resulted in the development of an Al concentration gradient, so that the critical level for reformation of a protective scale (C_{bb} in the model) was reached at the metal surface in the corner while the bulk Al content was still relatively high. Less Al depletion was measured at the opposite ends of the same specimens, suggesting that spallation was not a uniform process. While failure of the short parallelepipeds also initiated at specimen corners, there did not appear to be preferential initiation at a single corner. The corners and edges of all specimens showed signs of gross deformation, apparently from elongation in the axial (parallelepipeds) or radial (disc) direction, presumably as a result of creep of the substrate to relieve the compressive stress developed in the scale. The undulating metal-oxide interfaces formed on all specimens provided evidence of localized stress relief by creep of the alloy surface, likely occurring at temperature and driven by oxide growth stresses. Cracks observed in the outer scale surface over such undulations penetrated up to half the scale thickness but, as anticipated [15], there were no signs that these had led to scale spallation. Superimposition of the stresses from oxide-alloy expansion mismatch during cooling may have contributed to the growth of these undulations, and was probably the main driving force for gross deformation of the specimen ends. This study did not provide evidence of the times during the exposures when these phenomena initiated.

Finite element modeling has suggested that tensile stresses develop across the metal-oxide interface during cooling from temperature that can be sufficiently large to cause deformation at alloy corners [16]. Under conditions where the alloy undergoes work hardening, or exhibits perfectly plastic behavior, such deformation is calculated to take a similar form (but more symmetrical) to that observed here. ODS alloys exhibit significant work hardening, as well as a threshold stress above which failure in tension is rapid. The role in this process of the shape of the corners may also be considerable: modeling suggests that reducing the ratio of corner curvature to oxide thickness may lead to a change in stress state at the outer corner surface of the oxide, from compressive to tensile, as well as to the relocation of the maximum principal stress from the outer oxide surface to within the substrate.

As mentioned above, the form of the corner deformation on standard parallelepipeds typically was not symmetrical. A possible scenario for this is that, during cooling, the immediate alloy surface remains fixed in space (near its location at temperature) because it is locally pinned by the adherent oxide (which contracts less), forcing less-constrained alloy some distance beneath the interface to accommodate the stresses. This accommodation is manifested by preferential movement of the alloy at the specimen ends, where the difference in length (and, presumably, stress) between the major surface and the end surface results in preferential movement of the end surface, and asymmetrical deformation at the corner. The fact that the corners of the standard parallelepipeds were more susceptible to earlier or more persistent spallation than those on the other shapes tempts a correlation with a shape factor involving the maximum continuous length of specimen surface/scale (even though stress relief at the metal-oxide interface is likely to involve local phenomena). There are obviously further issues to consider, since stress relief may take different forms depending on scale thickness, alloy mechanical properties, and specific specimen shape, and so have different effects on scale spallation.

While for the short parallelepipeds and the discs it appeared that consumption of the Al content was quite uniform on all surfaces (even when small amounts of scale spallation occurred as in the case of the disc edges), these results cannot be interpreted to indicate that this condition continued until the Al content was essentially exhausted. In particular, the Cr profiles suggest that consumption of Cr had initiated at edges and corners of the discs (hence the observed early spallation), but not on the major faces. Unfortunately, it appeared that both short parallelepiped specimens examined had been oxidized past the point of initial breakaway, so that the measured Al profiles were not properly representative of those at the point of failure.

Ideally, in a specimen taken to the point of chemical breakaway, failure will occur when the activity the Al falls below that in equilibrium with Al_2O_3 , which is a very small value. In practice, an increase in the population of precipitates of alumina and AlN beneath the external scale immediately prior to failure is commonly observed for this alloy type [5,11]; the availability of Al to form these precipitates suggests that such a change occurred before the theoretical minimum Al activity was reached. This ultimate consumption of the remaining Al in the alloy, and the formation of Cr_2O_3 at the base of the scale, leads to the observed increase in the rate of mass gain and spallation of the scale on cool down. In all probability, the value of C_{Bb} is higher than the 0-0.001 value currently accepted for chemical failure, so that further measurements at sequential exposure times before the point of failure are needed to accurately fix its effective value.

If the Al concentration profile remains flat until the specimen undergoes chemical breakaway, as appeared to be likely for the disc specimens, then the Al content at the end of life (C_{Bb}) should be readily calculable from the mass change data. Fig. 9 shows the total mass change for the three shapes oxidized to failure recomputed in terms of Al consumption, assuming that only alumina was formed. The mass of scale spallation also is shown. The point at which the Al consumption curve obviously deviated to a higher rate was taken to indicate the point of breakdown, and was readily discerned for the disc and standard parallelepiped; for the short parallelepiped there was no distinct deviation, so that this point was taken to be that at which the rate of scale spallation sharply increased. The lifetimes determined in this way agree with those indicated in Fig. 1, and the apparent bulk values of C_{Bb} are compared to the measured values in Table 4. The good correspondence of the extrapolated remaining bulk Al level with those measured in the center of the failed, large parallelepiped specimen may be a reflection of the localized nature of the corner depletion of Al that led to failure. However, the large discrepancy between the extrapolated and measured values for the disc tend to confirm the suspicion that accelerated attack had already initiated at the point of deviation of the mass gain curve. The observed spallation of scale in large sheets from the major surfaces of the discs after cooling at the end of the test apparently was a result of general breakdown with continued exposure before removal from test.

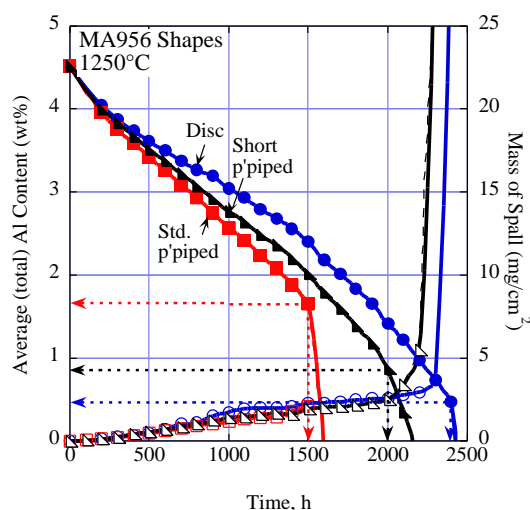


Figure 9. Oxidation kinetics plotted as Al consumption

Table 4. Summary of the average remaining Al levels at failure

Specimen	Life [kh]	Average Al Concentration [wt%]	
		Measured	From mass change
Standard p'piped	1.4-1.5	1.65	1.63
Short p'piped	2.0-2.1	0.1	0.85
Disc	2.3-2.4	0.1	0.46

Conclusions

The observation that standard parallelepiped-shaped specimens exhibited a significantly shorter time to breakaway oxidation than did short parallelepipeds and discs having the same thickness and V/A ratio has both mechanistic and practical implications. Overall, it appears that under the conditions of these tests, the oxidation behavior was in accordance with the processes described by the Al consumption-based modeling approach, but that failure was initiated by mechanical breakdown due to localized Al consumption by persistent scale spallation. The early failure of the standard parallelepipeds was due to the development of a local Al gradient, with the interface Al level in a corner falling below some critical value while the bulk Al level was 1.65-1.70%. If this behavior reflects an increasing inability to relieve the accumulated stresses between the scale and substrate with increasing physical length of continuous scale, it may be possible to devise a suitable shape factor that would allow the current modeling approach to account for the observed differences. For the discs, which did not develop obvious signs of breakaway oxidation despite an increase in mass gain immediately before removal from the test, failure appeared to initiate essentially simultaneously around the specimen peripheries. While a flat Al profile was measured (0-0.1% Al) even though voluminous scales had not formed, observations suggested that the actual value for C_{Bb} was somewhat higher.

Acknowledgements

This research was sponsored by the U.S. Department of Energy, Office of Fossil Energy, Advanced Research Materials Program, under Contract DE-AC05-00OR22725 with UT-Battelle, LLC. The authors would like to thank G. W. Garner, H. F. Longmire, and L. A. Walker for conducting the experimental work, and P. F. Tortorelli and S. J. Pawel for reviewing the manuscript.

References

- [1] I.G. Wright, B. A. Pint, C. G. McKamey, "ODS alloy development," Proc. 17th Annual Conference on Fossil Energy Materials, Baltimore, Maryland, April 22-24, 2003; see 'Conference Proceedings' at <http://www.netl.doe.gov/>
- [2] J.P. Wilbur, M.J. Bennett, and J.R. Nichols, *Mater. at High Temp.*, 17 (1), 125-132 (2000).
- [3] W.J. Quadakkers and M.J. Bennett, *Mat. Sci. Technology*, 10, 126-131 (1994).
- [4] W.J. Quadakkers and K. Bongartz, *Werkst. Korros.*, 45, 232-41 (1994).
- [5] G. Merceron, R. Molins, J.L. Strudel, I. Alliat, and L. Menneron, *Mater. Sci. Forum*, 369-372, 269-276 (2001).
- [6] I.G. Wright, B.A. Pint, C.S. Simpson and P.F. Tortorelli, *Mater. Sci. Forum*, 251-254, 195-204 (1997).
- [7] I.G. Wright, B. A. Pint, L. M. Hall, and P. F. Tortorelli, pp. 339-358 in *Lifetime Modelling of High-Temperature Corrosion Processes*, M. Schütze, W. J. Quadakkers, and J. R. Nicholls, Eds., EFC Publication No. 34, Maney Publishing (2001)
- [8] L. Maréchal, B. Lesage, A.M. Huntz, and R. Molins, *Oxdt. Metals*, 60 (1/2), 1-28 (2003).
- [9] J.R. Nicholls, M.J. Bennett, and R. Newton, poster at 5th International Conference on the Microscopy of Oxidation, Limerick, Ireland (2002).
- [10] B.A. Pint, L.R. Walker, and I. G. Wright, "Characterization of the Breakaway Al Content in Alumina-Forming Alloys," Proc. 5th International Conference on the Microscopy of Oxidation, Limerick, Ireland (2002).
- [11] H. Al-Badairy, G.J. Tatlock, and M. J. Bennett, *Mater. at High Temp.*, 17 (1), 102-107 (2000).
- [12] M. J. Bennett, H. Romary and J. B. Price, pp. 95-103 in *Heat Resistant Materials*, K. Natesan and D. J. Tillack, eds., ASM, Materials Park, Ohio (1991).
- [13] I.G. Wright, B. A. Pint, unpublished work.
- [14] N. Hiramatsu and F.H. Stott, *Oxdt. Metals*, 51, 479-94 (1999).
- [15] J.K. Wright, R.L. Williamson, D. Renusch, B. Veal, M. Grimsditch, P. Y. Hou, and R.M. Cannon, *Mat. Sci. & Eng.*, A262, 246-255 (1999).
- [16] J.K. Wright, R.L. Williamson, and R.M. Cannon, *Mat. Sci. & Eng.*, A338, 411-421 (1997).